VLA Scientific Memo. No. 171

Paired Array Calibration at the VLA

C.L. Carilli and M.A. Holdaway

National Radio Astronomy Observatory

Socorro, NM, 87801

M. Ishiguro

Nobeyama Radio Observatory, Japan

November 1, 1996

Abstract

We perform observational tests of the paired array calibration technique for correcting tropospheric phase variations at the VLA. Test observations were made in the C array with both the target and calibration arrays observing at 22 GHz, and in the D array with the target array observing at 43 GHz and the calibration array observing first at 8 GHz, then at 15 GHz. In the later case, the non-dispersive nature of tropospheric phase variations was employed to boot-strap solutions from low to high frequency. Results at all frequencies indicate that paired array calibration improves the rms phase variations relative to the tropospheric root phase structure function for most baselines in the C array, and the longer baselines in the D array, for typical weather conditions at the VLA.

1. Introduction

Paired array calibration involves phase calibration of a 'target' array of antennas using a separate 'calibration' array, where the target array is observing continuously a weak source of scientific interest while the calibration array is observing a nearby calibrator source (Holdaway 1992, Counselman et al. 1974, Asaki et al. 1996, Drashkik and Finkelstein 1979). In its simplest form paired array calibration implies applying the phase solutions from a calibration array antenna to the nearest target array antenna at each integration time. An improvement can be made by interpolating the solutions from a number of nearby calibration array antennas to a given target array antenna at each integration time. Ultimately, the discrete measurements in space and time of the phases from the calibration array could be incorporated into a physical model for the troposphere to solve for, and remove, the effects of the tropospheric phase screen on the target source as a function of time and space (Zheng 1985).

Paired array calibration was proposed by Holdaway (1992). Holdaway's analysis emphasized using the technique in the context of the MMA. The addition of a 7mm system at the VLA raises the issue of implementing calibration techniques designed to reduce tropospheric phase variations. In a previous memo we analyzed and tested the fast-switching phase calibration technique at the VLA (Carilli, Holdaway, and Sowinski 1996). Herein we present observations specifically designed to test the paired array phase calibration technique. Our application is limited to a linear interpolation of the measured phase screen from the two nearest calibration antennas to a given target array antenna at a specific instant in time. We also use the fact that the troposphere is a non-dispersive medium, *ie.* that the tropospheric contribution to the phase is linearly proportional to the observing frequency, to 'boot-strap' phase measurements at low frequency in the calibration array to higher frequency in the target array.

The observations were made on April 9, 1996 in the C array and June 30, 1996 in the D array.

2. Results: C Array at 22 GHz

The C array observations were all at 22 GHz, and entailed two subarrays of alternating antennas along each arm. One subarray pointed at the VLA calibrator 0423+418 and the second subarray pointed at the calibrator 0432+416. For analysis we define 0423+418 as the 'calibration source' and 0432+416 as the 'target source'.

Figure 1 shows the phase solutions over time for a few antennas from the two subarrays. The antennas at W16 and W4 are observing the source 0423+418 while the antennas at W18 and W6 are observing 0432+416. For adjacent pairs of antennas W16-W18 and W6-W4 the temporal variations in the phase track each-other very closely. This close relationship for phase variations between the two subarrays is the signature that the primary phase variations are tropospheric in origin, and are correlated on relevant timescales and baseline lengths.

Note however that while the temporal variations for neighboring antennas track each other very well, the mean phase over the observed time range is very different between the antennas. This phase off-set is primarily due to the VLA electronics and/or optics, and should be slowly varying (the original specifications for the VLA electronics indicate an RMS tolerance of up to 1^o phase variation per GHz, mostly due to long-timescale thermal effects). Before interpolating phase solutions from the calibration array to the target array one must first determine, and remove, these electronic phase terms. The method we employ to determine this electronic phase off-set is to calculate the mean phase for a given antenna over the full integration period of about 30 min.

The results are demonstrated in Figure 2. Figure 2a shows the calculated phases along the north arm of the array for a given 30 sec record at 0:45 IAT for both subarrays. Figure 2b shows the corresponding phases after removal of the mean electronic phase for each antenna. The phase variations along the arm in Figure 2a are essentially random, i.e. with a peak-to-peak variation close to 360°. The phase variations in Figure 2b show a smooth change along the arm, with phase difference increasing with baseline length to a maximum of 40° for the furthest antenna. This behavior is indicative of tropospheric phase variations. Moreover, the smooth residual curve in Figure 2b for data from the two subarrays lends hope to the idea that the tropospheric phase contribution can be interpolated from the calibration source array to the target source array, after application of the electronic phase off-set in each subarray. In practice, this electronic phase off-set can be determined by having both subarrays observe the same calibrator every 30 minutes or so. We have performed tests which show that this electronic phase off-set is stable on timescales of hours, and does not vary with source changes, at least for nearby sources. Also, calibration every 30 minutes allows for a solution of the (slowly varying) antenna gains – a term which is not calibrated in the phase transfer process described below.

A data set of visibilities from the two subarrays was generated with the electronic phase off-set applied. The residual phase variations were then determined every 30 seconds for the calibration array. These solutions were then applied to the target array antennas by interpolating the solutions from the two calibration array antennas which bracket the target array antenna along an arm of the array. As a check on these interpolated solutions, the 'true' phase values for the target array were determined through self calibration on 0432+416, with a 30 second averaging time. A comparison between the true phase solutions for the target array and the phase solutions interpolated to the target array from the calibration array is shown in Figure 3.

To determine the residual errors in the interpolated phases, the calibrated data from

the target array (ie. with interpolated solutions from the calibration array applied) were then self-calibrated. The residual phase corrections are plotted for a few antennas in Figure 4. Typical peak-to-peak residual corrections are $\leq 50^o$.

A quantitative measure of the effects of paired array calibration can be seen in the root phase structure function plotted in Figure 5. The open triangles show the tropospheric root structure function for the given observing day, as determined from the data with only the mean phase calibration (30 min averaging) applied. The shape of this function is well fit by a power-law in rms phase versus baseline length with index 0.65, consistent with Kolmogorov turbulence theory on baselines shorter than 1 km (Sramek 1992). The rms magnitude of 35^o on a baseline of 1000 m is slightly higher than the expected value of about 25^o on a typical summer evening at the VLA (Carilli etal. 1996). The stars in Figure 5 correspond to the 'noise floor' for the phase measurements, as determined by calculating the root structure function from self-calibrated data. The solid squares in Figure 5 show the root structure function for the data with paired array calibration applied. The residual rms values are about 10^o on short baselines, and increase very slowly with baseline length. These data indicate a significant improvement in RMS phase fluctuations after application of paired array calibration for baselines longer than about 300m. The increased noise floor for the paired array calibrated data relative to self-calibration indicates residual short-timescale phase differences which do not replicated between the target and calibration arrays. We discuss the origin of these fluctuations in more detail in Section 4.

The results of paired array calibration can be seen on the images in Figure 6. Figure 6 A shows the image made from data with only the mean electronic phase off-set applied. Figure 6 B shows the image after paired-array calibration, and Figure 6 C shows the image after self-calibration with a 30 sec averaging time. The peak surface brightnesses are 0.79 Jy, 0.99 Jy, and 1.02 Jy, respectively, and the peak side-lobes in each image are 59 mJy, 14 mJy, and 2.8 mJy, respectively. Hence, calibrating every 30 minutes results in a significant

loss in coherence: the peak surface brightness is only 80% that expected, while the image after application of paired array calibration has 98% coherence. The image fidelity $\equiv (\frac{peak\ surface\ brightness}{peak\ side-lobe})$ increase from 13 in Figure 6 A, to 70 in Figure 6 B, and to 360 in Figure 6 C.

3. D Array: Bootstrapping from 8 GHz and 15 GHz to 43 GHz

The paired array technique has the advantage that for the target array no time is spent moving or calibrating. On the other hand, since half the antennas must be used for calibration, the loss in correlation products implies an increase in noise by a factor two over a continuous integration with the full array. In general then, fast switching will be preferred over paired array calibration for situations when the duty cycle $\equiv \frac{on-source\ time}{total\ observing\ time} > 25\%$. However, the VLA has the specific limitation that only 13 antennas are currently out-fitted with 43 GHz receivers, leaving the rest of the antennas free for phase calibration. The goal then is to test if phase calibration can be performed at a lower frequency and applied at 43 GHz using the non-dispersive nature of the tropospheric phase fluctuations.

Test observations were made on July 29, 1996 with the VLA in the D configuration. Observations were made using two sub-arrays: one involving 12 antennas with 43 GHz receivers and the second involving 14 antennas at other frequencies. The antenna locations for the two subarrays are listed in Figure 7. A period of 60 minutes was spent with the second sub-array observing at 8 GHz, and a second period of 30 minutes was spent with the second sub-array observing at 15 GHz. The source observed at 43 GHz (which we designate the 'target-source') was the VLA calibrator 0112-017. The source observed at the other frequencies (the 'calibration source') was the VLA calibrator 0111+021.

One difficulty encountered when using the paired array calibration technique at the VLA is that the array lay-out is not ideal. The paired array phase calibration technique will

work best when the calibration array antennas are fully interspersed with the target array antennas (ie. every-other station). Such a demand on the antenna placements may conflict with other constraints, such as best UV coverage. Also, the spacings between antennas in the A and B arrays are large ($\geq$ 1 km). The nominal expected tropospheric phase noise on such baselines are expected to be $\geq 30^{o}$ at 43 GHz, even in good conditions. While interpolation of solutions from two calibration array antennas which bracket the target array antenna will reduce the residual phase noise below this value, we expect that paired array calibration may only be viable in the smaller arrays.

The antenna locations for the two sub-arrays in our D configuration observations are listed in Figure 7. Only along the west arm are the target array and calibration array antennas properly interspersed. Along the east and north arm there are a number of places where target array antennas have only one neighboring calibration array antenna.

The calibration process was similar to that described in section 2 above. First the mean electronic phase off-set was removed for both the target and calibration arrays by applying self-calibration solutions averaged over 30 minutes. The calibration array data were then self-calibrated in phase with an averaging time of 30 seconds. These phase solutions were then interpolated from the closest two calibration antennas to each target array antenna, scaled by the ratio of frequencies, and applied to the target array. The results for antennas along the west arm are shown in Figure 8. Figure 8 A shows the 'true solutions' for the target array, as determined by self-calibration on 0112-017. Figure 8 B shows the 'paired array solutions,' i.e. the phases interpolated from the calibration array to the target array, scaled by a factor $= \frac{43}{15} = 2.9$. Figure 8C shows the residual phase corrections after application of the paired array phases as determined by subsequent self-calibration.

In many regions there is good agreement between the phase variations as determined from the paired array solutions and from the true solutions. Examples include the big

phase jump at 12:33 in W8 and W6, and the phase dip at the beginning of the observation on both W8 and W6. However, there are times when the paired array solutions differ significantly from the true solutions, eg. the phase dip at 12:22 in the paired array solutions does not appear with comparable strength in the true solutions, and the phase dip at 12:28 seen in the true solutions does not replicate in the paired array solutions. Also, at times where there are large gradients the shape of the gradients do not replicated exactly.

The impact of these differences can be seen in the residual phase corrections after application of the paired array solutions, as shown in the subsequent self-calibration solutions in Figure 8C. While the large phase change on antennas W8 and W6 at 12:33 seems to be removed, there are other residual corrections (eg. at 12:22) at the level of about 50^o on timescales of a few minutes. Also, there seems to a be long term drift of about 50^o in phase which is not removed in this process.

These effects can also be seen in Figure 9, which shows the observed phases versus time for two similar baselines along the west arm: W8-W4 at 43 GHz and W9-W5 at 8 GHz. While there are common features in both plots, eg. the large dips in phase at 12:57 and 13:11, and the increases at 13:02 and 13:07, there are significant differences: the large increase in phase at 12:51 does not replicate in the 8 GHz data, the dip in phase at 13:24 at 8 GHz is not seen at 43 GHz, and the slow rise in phase between 13:30 and 13:40 at 43 GHz does not occur at 8 GHz.

Again, a quantitative measure of the effects of paired array calibration can be seen in the root phase structure function plotted in Figure 10. The open triangles show the tropospheric root structure function for the given observing day, as determined from the data with only the mean phase calibration (30 min averaging) applied. Again, the shape of this function is well fit by a power-law in rms phase versus baseline length with index 0.65, consistent with Kolmogorov turbulence theory on baselines shorter than 1 km. The rms

magnitude of 25° on a baseline of 400m is slightly higher than the expected value of about 17° on a typical summer evening at the VLA (Carilli etal. 1996). The stars in Figure 10 correspond to the noise floor for the phase measurements, as determined by calculating the root structure function from self-calibrated data. The solid squares in Figure 10 show the root structure function for the data with paired array calibration applied, with solutions boot-strapped from 15 GHz to 43 GHz. The residual rms values are about 20° on short baselines, and increase slowly with increasing baseline length.

A comparable plot from 8 GHz paired array calibration data is shown in Figure 11. The results at 8 GHz are similar to those obtained at 15 GHz, with the one difference being that at 8 GHz the rms residuals parallel the root structure function for short baselines, while at 15 GHz the residuals remain roughly constant for all baselines, and hence exceed the root structure function for short baselines.

The effects of paired array calibration on the images is shown in Figure 12. Figure 12 A shows an image made after applying only the mean phase calibration (30 min average). Figure 12 B shows the result after applying the paired array calibration. The peak surface brightnesses are 920 mJy/beam and 940 mJy/beam, respectively, while the peak side-lobes are 104 mJy and 76 mJy. respectively. Overall, the application of the paired array calibration has made a slight improvement in the image coherence by 3%, and a modest improvement in the image fidelity by about 30%. We expect that in the C array the improvement using paired array calibration will be more pronounced, since the rms residuals after paired antenna calibration will increase much more slowly with increasing baseline length than the root phase structure function, as was demonstrated in the C array at 22 GHz (see Section 2).

4. Discussion

Comparing the data in Figures 10 and 11 with those found at 22 GHz (Figure 5), we see similar results: paired array calibration improves the rms phase variations relative to the tropospheric root phase structure function for baselines longer than about 300m, but it also increases the noise floor substantially over the short timescale self-calibration results. Unfortunately the longest baselines in D array at 43 GHz were only about 700m, hence the improvement in the D array images after paired array calibration is less dramatic than was seen for the C array data. Note that a baseline length of 300 m is not a 'magic' value, but simply corresponds to the distance at which the residual phase noise crosses the tropospheric phase noise for both these particular observations. This crossing point will vary under different weather conditions.

The principal remaining question is: what causes the increase in phase noise after applying paired array calibration relative to self-calibration? Clearly, a contribution will come from the the residual effect of the troposphere. One contributing factor is the distance between the references antennas for the two arrays $\approx$ 40m, for which rms errors $\approx 5^o$ are expected using the root phase structure function as defined by the triangles in Figure 10. A second contributing factor is the distance between the various target and calibration array antennas. This distance increases from about 40m for the inner antennas to about 90m for the outer antennas. The expected rms error on a 90m baseline is $\approx 9^o$. A third factor is the distance in the troposphere between the target source and the calibration source. For the D array data this angular distance was 4^o, corresponding to a physical distance in the troposphere of $70\frac{h}{1km}$ m, where h is the height of the troposphere in km. The expected rms error on a 70m baseline is $\approx 7^o$. Taking the rss of these three factors, and including the noise floor value of 5^o seen in the self-calibrated data, leads to an expected rms residual of 11^o on the shortest baselines, and 13^o on the longest spacings. These residuals are

somewhat lower than the observed value of about 20°, suggesting that either the height of the troposphere was about 3km during the observations, or that there were residual, short-timescale electronic phase variations which did not replicate between the arrays. The required magnitude of this phase 'jitter' increases roughly as 0.5^{o} GHz^{-1}.

A second, related question is: why do the 8 GHz residuals parallel the root structure function on short baselines, while the 22 GHz residuals remain roughly constant to the shortest baseline? Unfortunately, the C array data does not provide insight into this question due to lack of the shortest spacings. Further tests are planned to investigate this question.

Overall, the current tests indicate that paired array calibration should be a useful technique in the C array, and perhaps in the D array under certain (bad) weather conditions. A future improvement may come from a robust modeling algorithm involving a reasonable physical model for the troposphere and employing all the point measurements of the tropospheric phase from the entire array as a function of space and time. Such an algorithm may be able to fit-out any electronic variations, and return the tropospheric contribution to the phase alone.

References

Asaki, Y., Saito, M., Kawabe, R., Morita, K., Sasao, T. 1996, Radio Science, in press

Carilli, C. and Holdaway, M. 1996, VLA Scientific Memo. No. 169

Coulman, C.E. 1990, in *Radio Astronomical Seeing*, eds. J. Baldwin and S. Wang, (Pergamon: New York), p. 11

Counselman, C.C. et al. 1974, Phys. Rev. Lett., 33, 1621

Draskikh, A.F. and Finkelstein, A.M. 1979, Astrophy. Space Sci., 60, 251

Holdaway, M.A. 1992, MMA Memo. No. 84

Sramek, R. 1990, in *Radio Astronomical Seeing*, eds. J. Baldwin and S. Wang, (Pergamon: New York), p. 21

Zheng, Y. 1985, Ph.D. Thesis, Iowa State University.

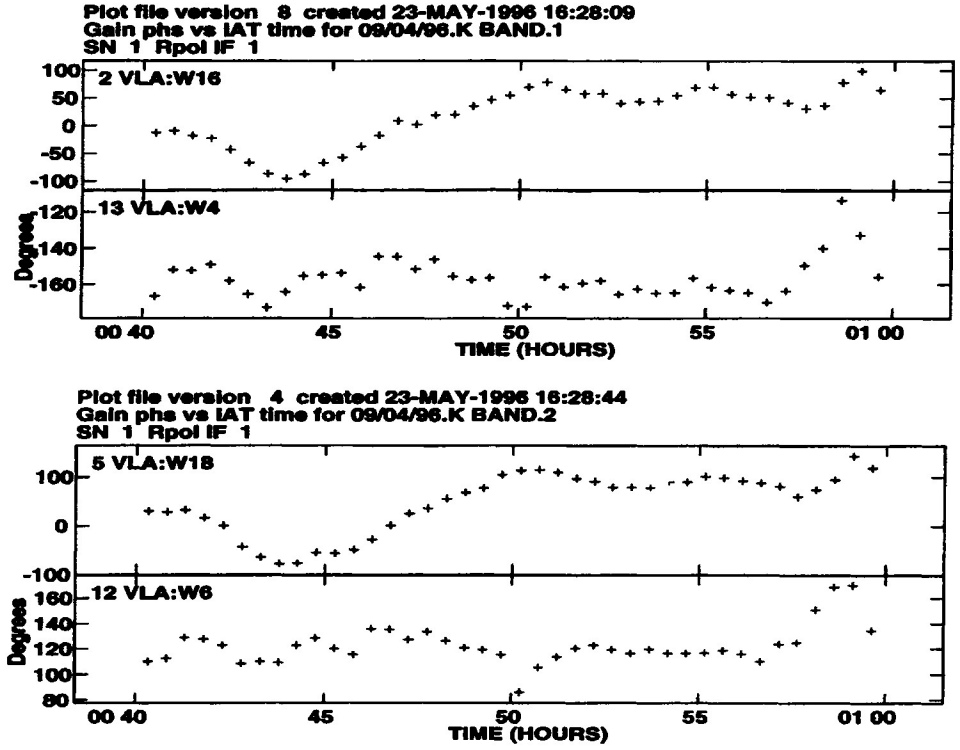

Fig. 1.— The top figure shows phase solutions versus time for two antennas along the west arm in a subarray observing 0423+418. The bottom figure shows the phase solutions over the same time for two antennas in the second subarray observing source 0432+416. Antennas 5 and 2 are adjacent, as are antennas 12 and 13

0

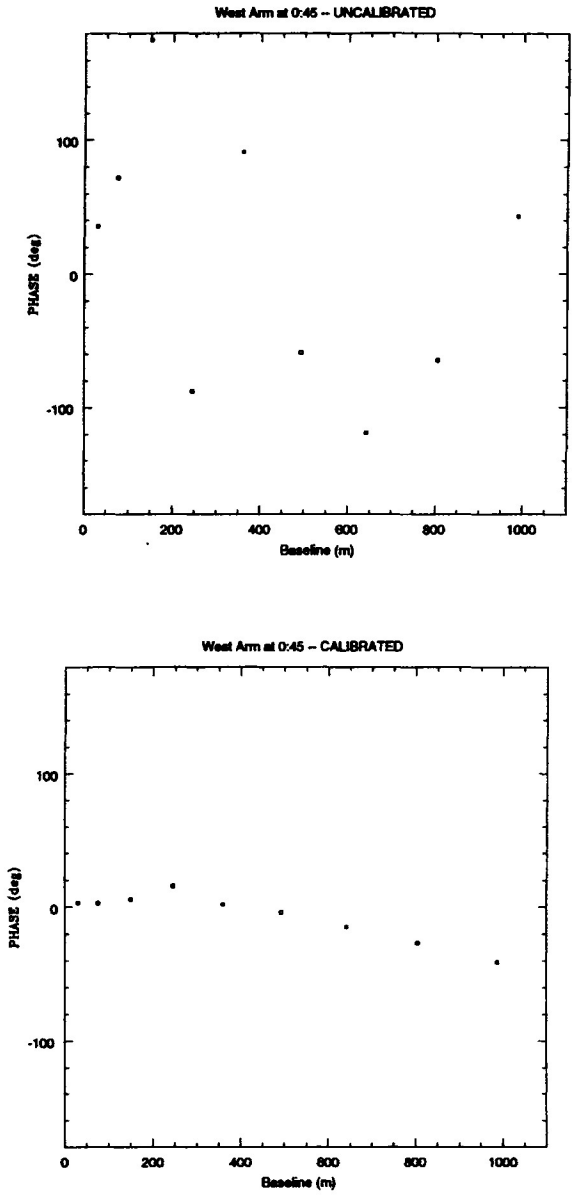

Fig. 2.— The top figure shows phase solutions for antennas along the west arm for a single 30sec interval at 0:45 IAT. The solid squares are in the calibration array (observing 0423+418) while the open squares are in the target array (observing 0432+416). The bottom figure shows the same phase solutions after application of the mean electronic phase.

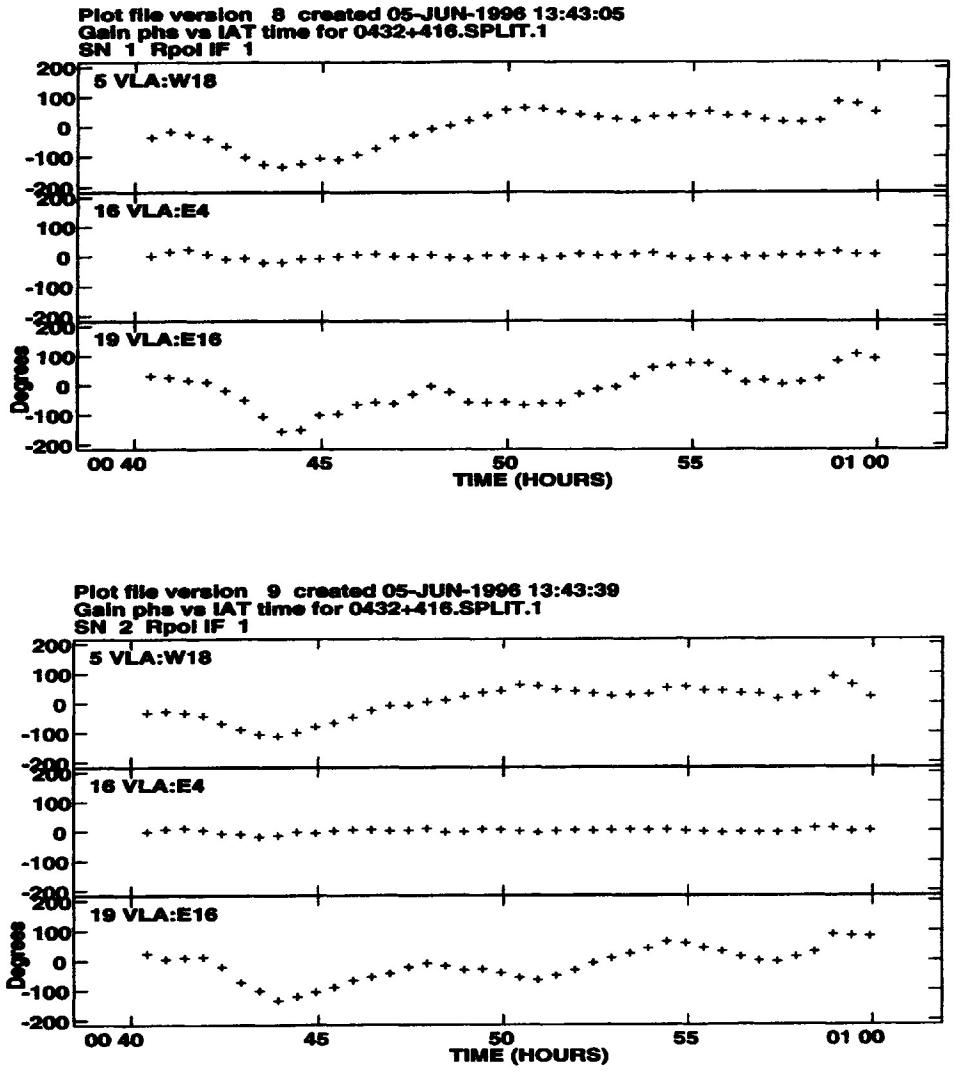

Fig. 3.— The top figure shows phase solutions versus time for self-calibration on the 'target' source 0432+416. The bottom figure shows the solutions as determined by the paired array technique using the calibration array.

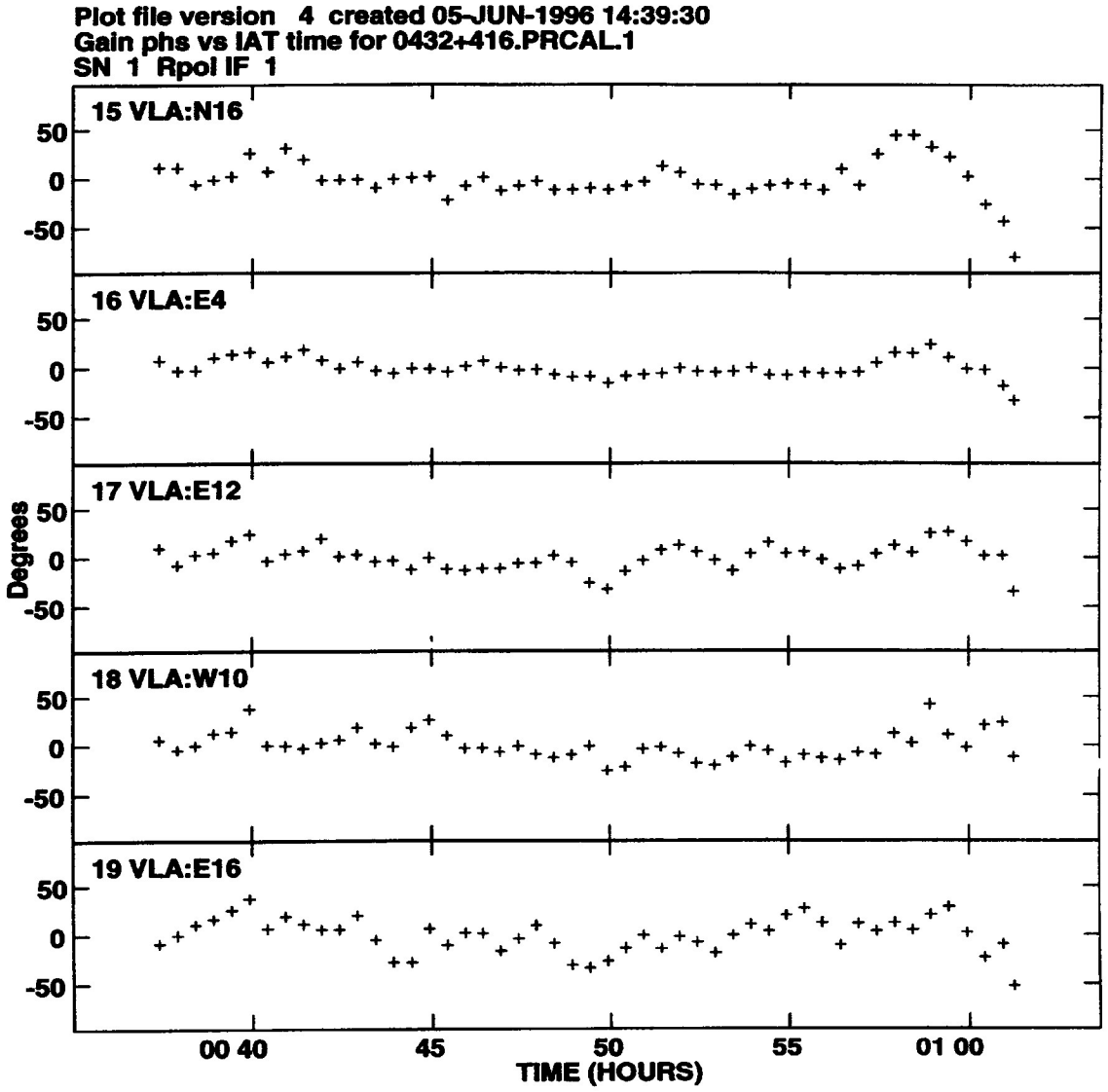

Fig. 4.— Residual phase corrections (determined from self-calibration on 0432+416) after application of the paired array phase solutions from the calibration array.

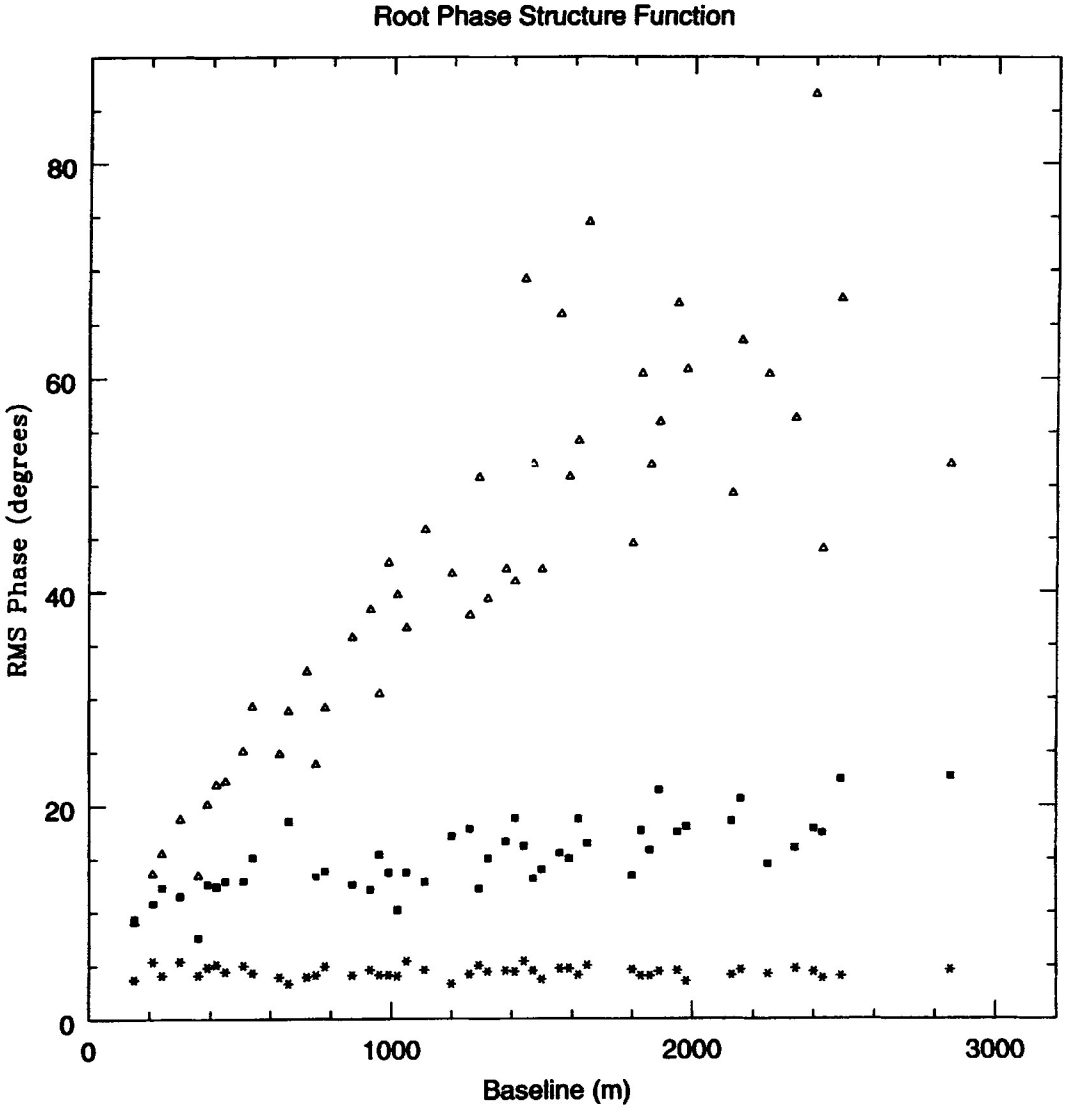

Fig. 5.— The open triangles show the root phase structure function for the data at 22 GHz on the target source 0432+416 as determined from data with only a mean (30 minute averaged) phase self-calibration applied. The stars show the structure function after application of self-calibration with 30 second averaging. The solid squares show the structure function after application of paired array calibration also at 22 GHz and again with 30 second averaging.

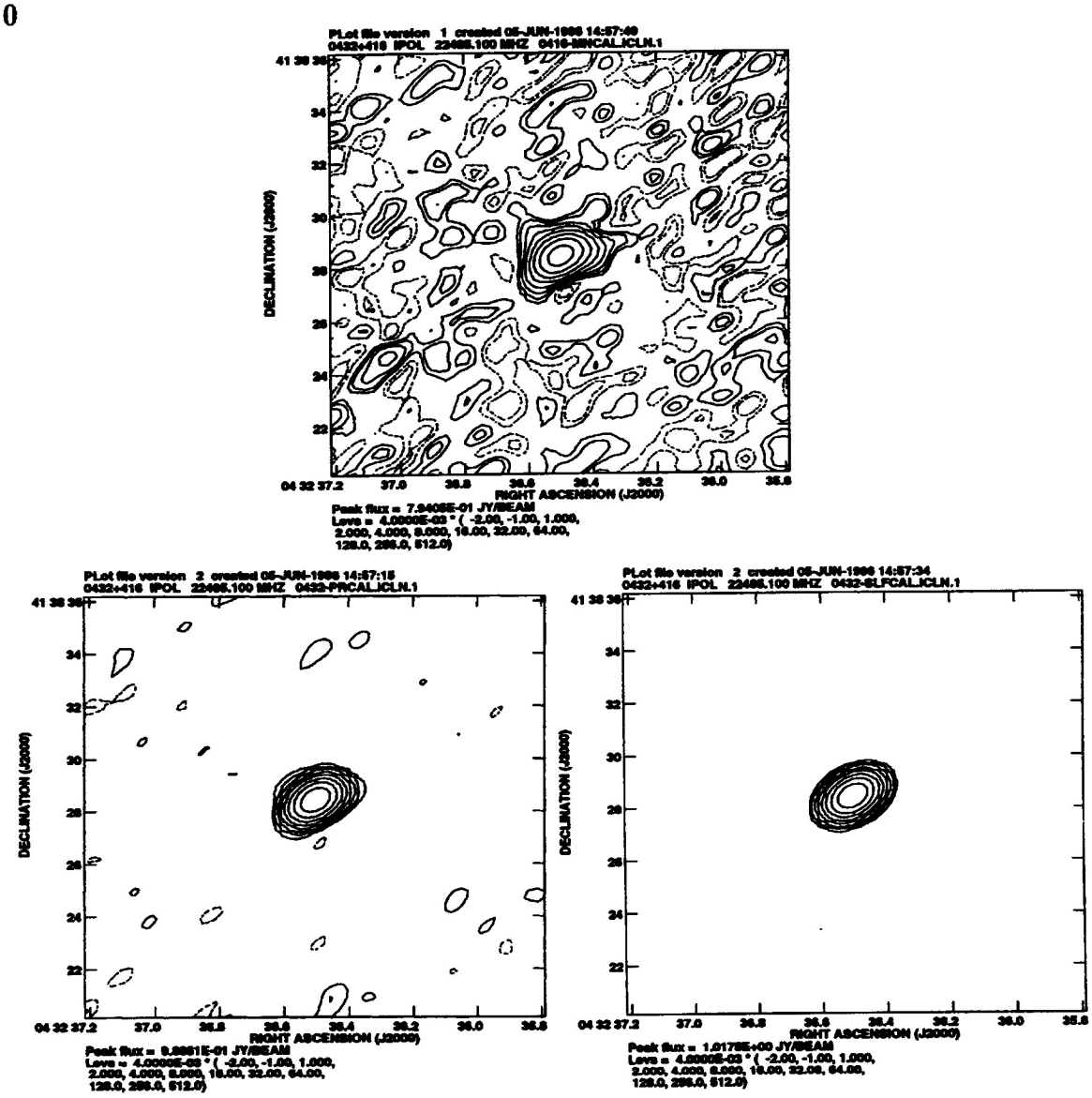

Fig. 6.— The top figure shows an image of 0432+416 generated from data with only the mean electronic phase calibration applied. The lower left image has had the paired array calibration from the calibration array applied, and the lower right image has been self-calibrated.

43 GHz:

N1(14) N3(20) N4(11) N8(27)

W2(25) W4(13) W6(12) W8(8)

E1(6) E4(16) E7(22) E8(4)

8GHz and 15 GHz:

N2(24) N5(23) N6(9) N7(15) N9(1)

W1(18) W3(10) W5(28) W7(2) W9(5)

E2(7) E3(17) E5(26) E6(19) E9(21)

Fig. 7.— The antenna placements for the two subarrays used in the D array observations. The target array at 43 GHz is listed on the top, while the the calibration array (8 GHz and 15 GHz) is listed on the bottom. Pad numbers and antennas numbers are listed for the North arm (N), the West arm (W) and the East arm (E), respectively.

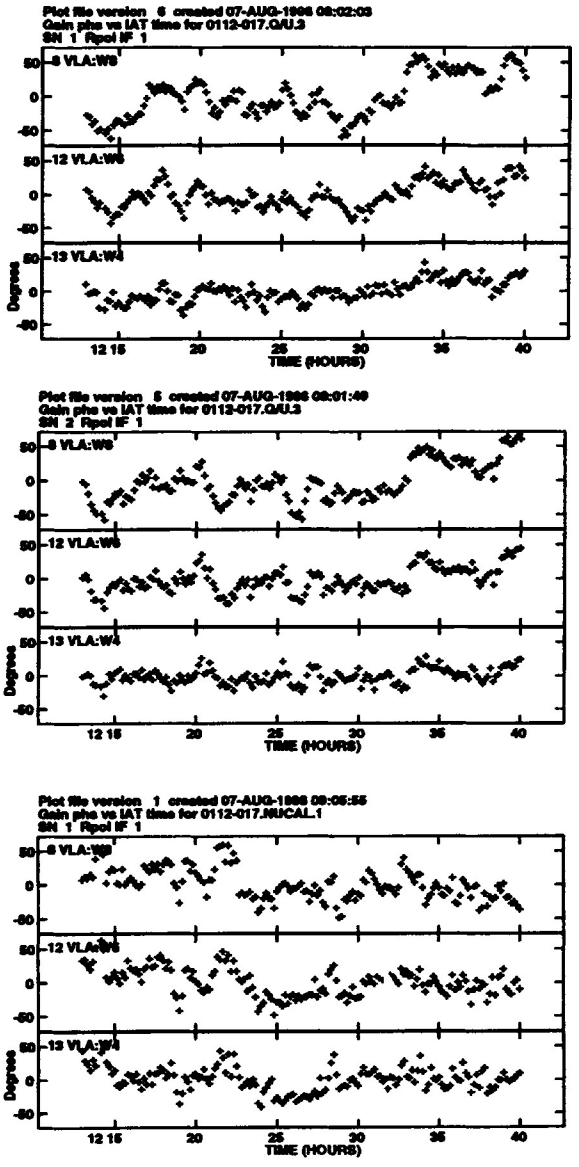

Fig. 8.— The top figure shows antenna-based phase solutions from self-calibration at 43 GHz with a 30 second averaging time for the target source 0112-017 for antennas along the West arm. The middle figure shows the corresponding solutions from paired array calibration, when boot-strapping solutions from 15 GHz to 43 GHz. In both cases the mean 'electronic phase' has first been removed via self-calibration with a 30 minute averaging time. The bottom frame shows the residual corrections at 43 GHz after application of the paired array solutions.

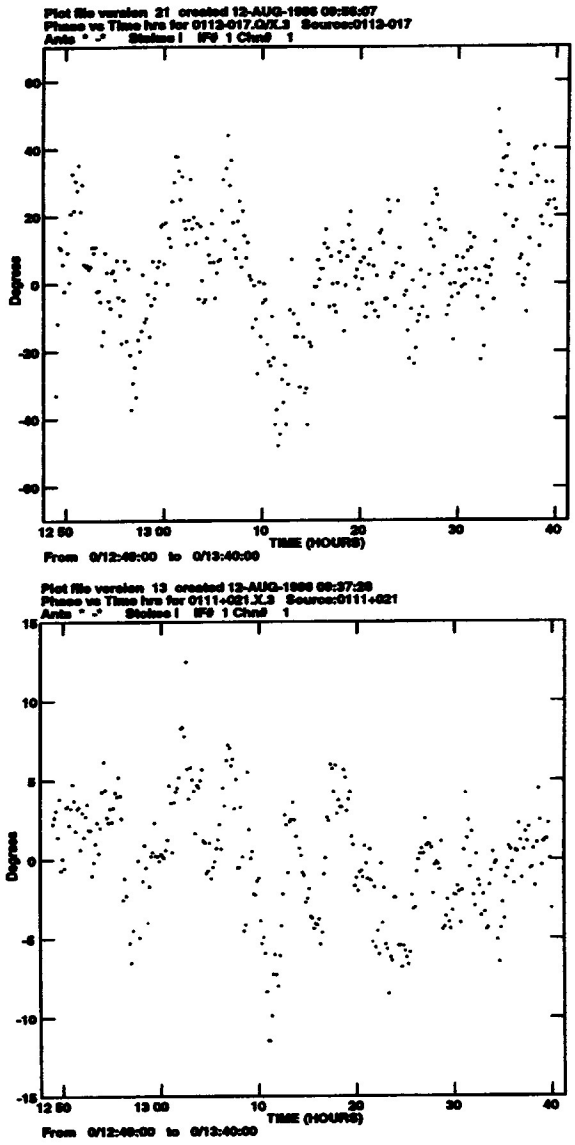

Fig. 9.— The top frame shows interferometer phase for the W8-W4 baseline versus time at 43 GHz while observing the source 0112-017. The bottom frame shows interferometer phase for the same time range for the W5-W9 baseline observing the source 0111+021 at 8 GHz. Note that in both cases a mean phase off-set has been removed via self-calibration with a 30 minute averaging time, and that the vertical scales differ by a factor 4.5.

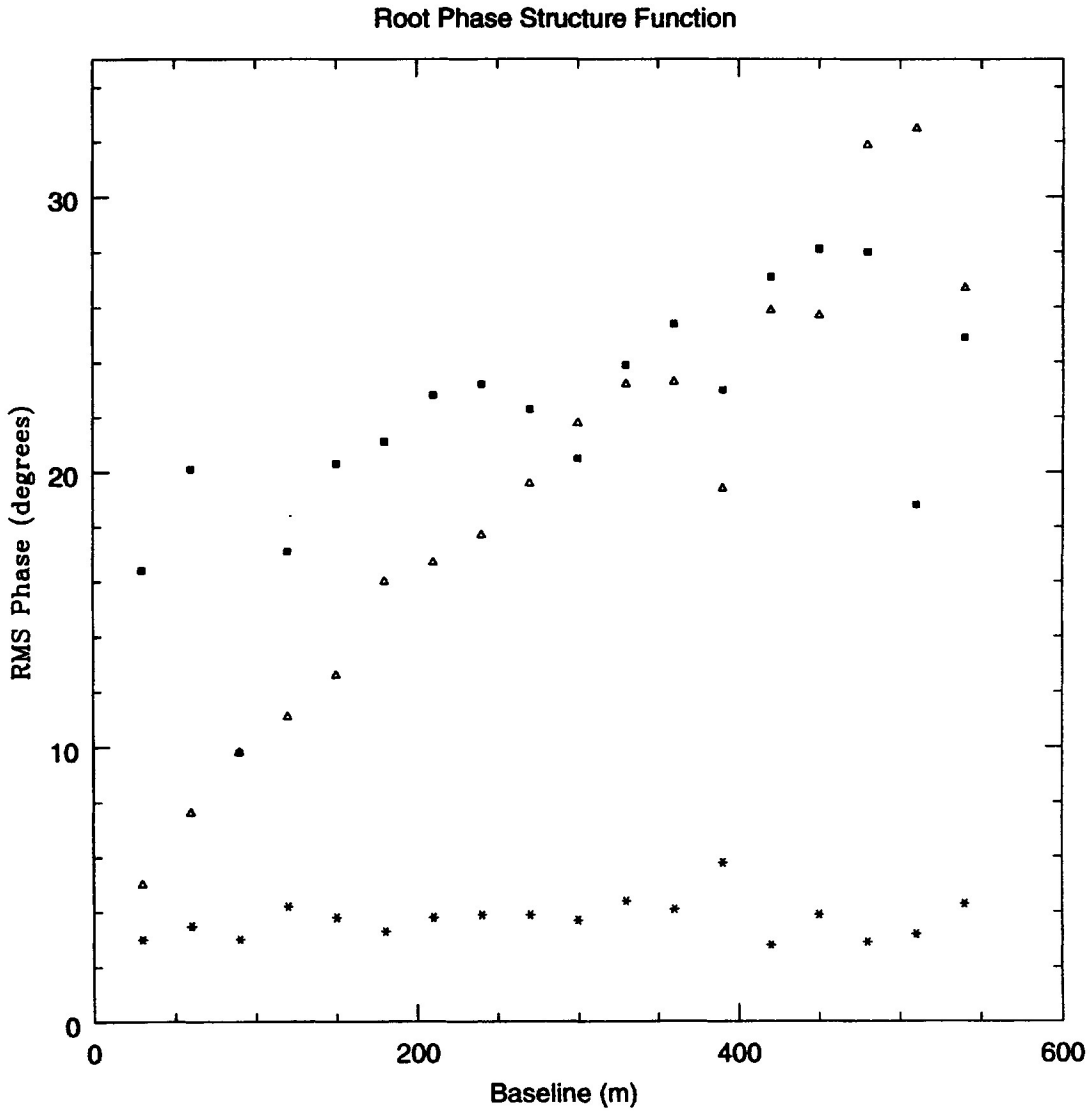

Fig. 10.— The solid squares show the root phase structure function at 43 GHz after application of paired array calibration, with solutions boot-strapped from 15 GHz and using 30 second averaging. The open triangles show the root phase structure function for the data at 43 GHz on the target source 0112-017 as determined from data with only a mean (30 minute averaged) phase self-calibration applied. The stars show the structure function after application of self-calibration with 30 second averaging.

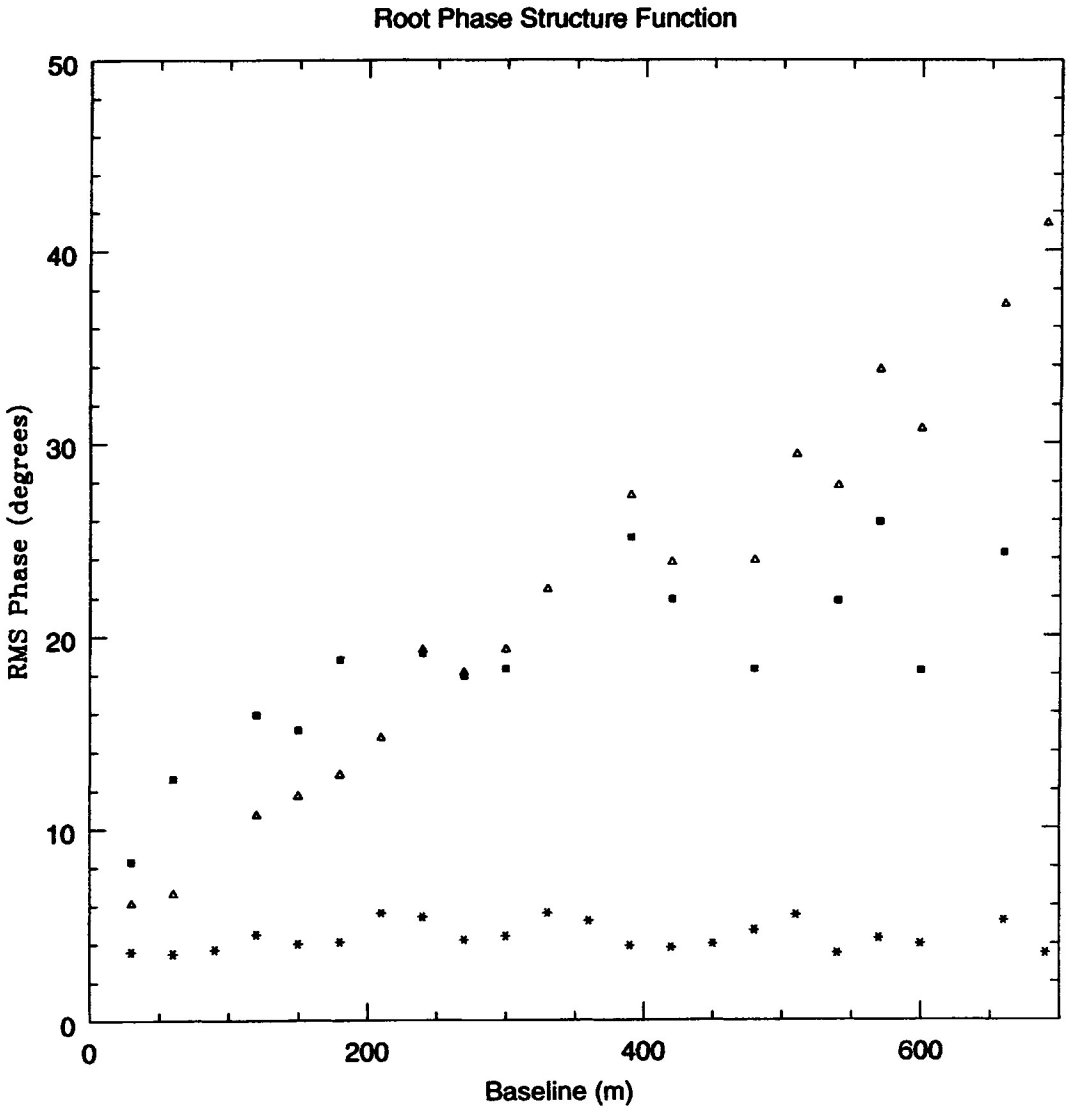

Fig. 11.— The solid squares show the root phase structure function at 43 GHz after application of paired array calibration, with solutions boot-strapped from 8 GHz and using 30 second averaging. The open triangles show the root phase structure function for the data at 43 GHz on the target source 0112-017 as determined from data with only a mean (30 minute averaged) phase self-calibration applied. The stars show the structure function after application of self-calibration with 30 second averaging.

0

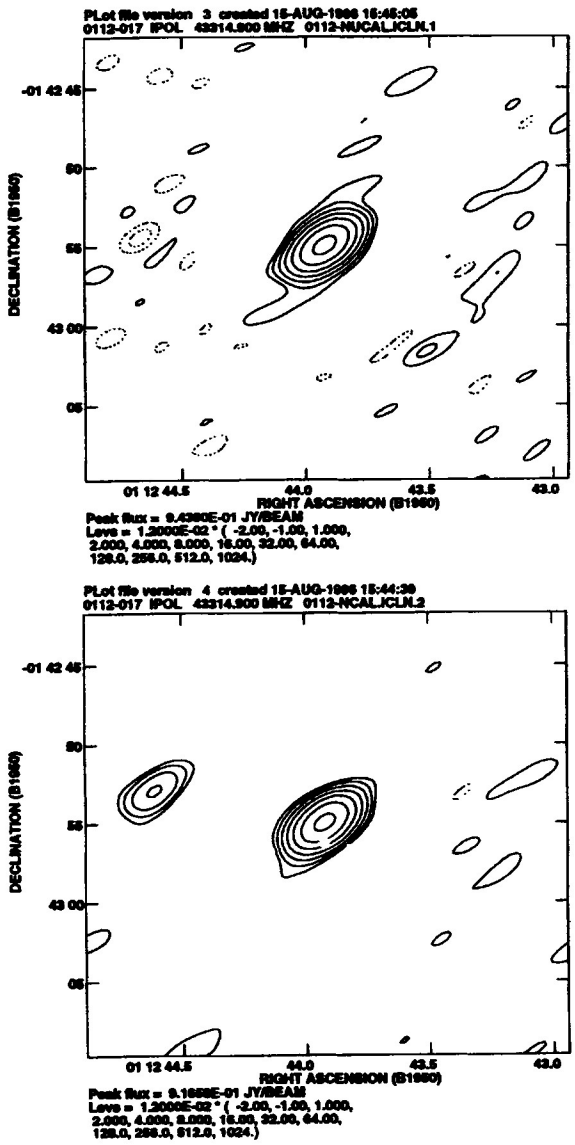

Fig. 12.— The top figure shows an image of 0112-017 generated from data with only the mean electronic phase calibration applied. The lower left image has had the paired array calibration applied for data taken when the calibration array was observing at 15 GHz.